Control Engineering Practice 17 (2009) 1405–1414

Contents lists available at ScienceDirect

Control Engineering Practice

journal homepage: www.elsevier.com/locate/conengprac

Multi-path nonlinear dynamic compensation for rudder roll stabilization

John F. O'Brien *

Department of Electrical Engineering, University of Wyoming, Department 3295 1000 E. University Avenue, Laramie, WY 82070, USA

ARTICLE INFO

Article history:
Received 11 September 2008
Accepted 15 June 2009
Available online 26 July 2009

Keywords:
Absolute stability
Marine systems
Nonlinear dynamic compensation
Non-minimum phase
Nyquist-stable

ABSTRACT

The design of rudder roll stabilizers (RRS) for ships is complicated by yaw-axis coupling, non-minimum phase shift, and the angle and rate limits of the rudder. These saturations tend to limit the available feedback and restrict RRS implementation to vessels with very fast rudders. This paper describes the application of a Nyquist-stable RRS with a multiple feedback path nonlinear dynamic compensator to provide high performance with *slower steering mechanisms* used on larger vessels. The restrictive sufficient condition of absolute stability is satisfied for angle or rate saturation. Computer simulation results are included to show the efficacy of the approach.

1. Introduction

Motion on a ship's roll axis can have several detrimental effects including cargo damage, reductions in crew effectiveness and increased pilot workload in helicopter landings (Faltinsen, 1990). Methods to attenuate this effect include the usage of fin stabilizers, bilge keels, anti-rolling tanks and rudder roll stabilizers (RRS) (Fossen, 1994). In contrast to other methods of roll motion reduction, RRS is attractive in that it does not require additional articulating surfaces to be incorporated into the ship design. Drawbacks of RRS include the lack of performance at low speed and severe feedback limitations of the roll control loop. For an RRS system, the rudder is the actuator in a two output (roll and heading) system coupled by rudder-induced sway. Thus, the yaw and roll loops must be designed with sufficient bandwidth separation, which has a limiting effect on available roll control feedback. The roll plant is typically non-minimum phase (exhibits phase lag in excess of that from the Bode phase-gain formula) (Goodwin, Perez, Seron, & Tzeng, 2000), a characteristic in this application that increases the sensitivity of the closed loop system at low frequency. Another substantial limitation is the rudder mechanism itself, which is limited in maximum angle and angle rate. An excellent treatment of this issue is found in Roberts (1993). Effective RRS systems must carefully take into account these limitations in the design process.

Excellent research in the area of active roll stabilization is readily found in the literature. Pole placement is used in Fossen (1994) for RRS and yaw controller design that provides 66% roll reduction. Switched proportional-integral-differential (PID) control of the rudder and fin stabilizers are used in Engeln, Koshkouei, Roberts, and Burnham (2004). Classical, optimal and robust control theory is employed in Sharif, Roberts, and Sutton (1996) to provide roll stabilization with $30^\circ\,s^{-1}$ fins and a $6^\circ\,s^{-1}$ rudder. Model predictive control with an effective angle of attack constraint is used to prevent dynamic stall of fin stabilizers in Perez and Goodwin (2007). Several automated gain tuning algorithms to improve the performance of rudder roll stabilization controllers in saturation have been suggested, including the automatic gain controller (AGC) (van der Klugt, 1987) and the time-varying gain reduction (TGR) algorithm (Laudval & Fossen, 1998). Model predictive control is applied to the rudder roll problem in Perez (2005). Neural nets using internal model control (IMC) is investigated in Alarcin (2007) using fin stabilizers to provide 94% roll angle reduction. A third-order controller for a fin stabilizer roll reduction system in reported in Tzeng and Wu (2000) that applies a maximum of 38 dB of feedback. In Majecki, Katebi, and Grimble (2006), generalized minimum variance control is used with 40 and $20^\circ\,s^{-1}$ rudder to provide a maximum of 25 dB of feedback, resulting in 84% roll reduction.

Given the severe limitations of the ship dynamics and the rudder, the goal of increasing RRS performance is challenging. Boosting feedback over a fixed frequency interval improves performance, but can threaten stability when the rudder saturates. Clearly performance improvement cannot be achieved by linear control alone. A strategy of combined linear and nonlinear compensation to provide large feedback and stability in saturation is indicated for the RRS application. This involves high-order loop shaping to provide large feedback over the frequency interval of interest, and the development of a nonlinear dynamic compensator (NDC) to provide absolute stability (AS) when the system has a sector nonlinearity in the loop. A high-order rudder roll controller with nonlinear dynamic compensation for rudder angle saturation provides more than 85% roll reduction to a ship with a high performance rudder in O'Brien (2007). While the controller

* Fax: +1 307 766 2279.
E-mail address: obrienj@uwyo.edu

0967-0661/$ - see front matter © 2009 Elsevier Ltd. All rights reserved.
doi:10.1016/j.conengprac.2009.06.008

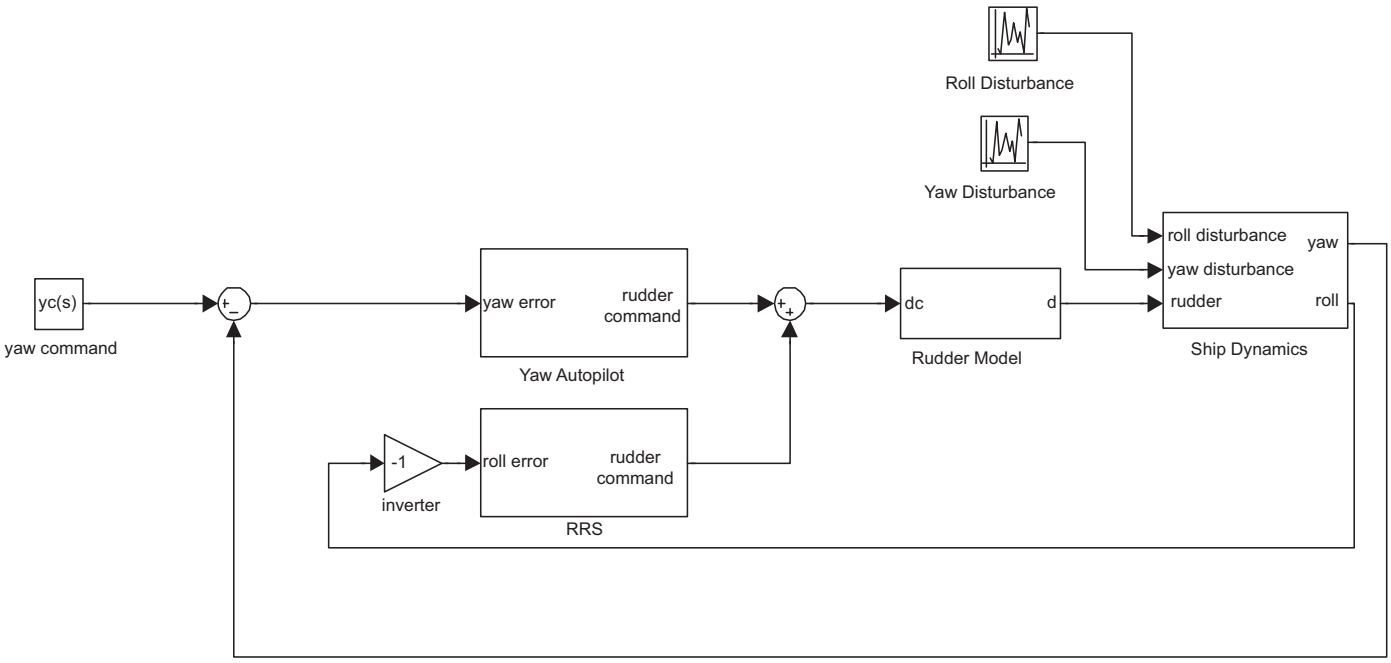

Fig. 1. The combined heading and rudder roll stabilization (RRS) control system.

has large feedback, it is absolutely stable only in angle saturation, and thus is applicable only for very high performance steering machines. It is critical that the effectiveness of this technology be shown for lower rudder bandwidth applications involving slower rudders that are implemented on larger vessels. This requires feedback adjustments in both rudder angle and rate saturation conditions. This paper presents a novel design using NDC with multiple feedback paths that provides improved performance over previously published designs and satisfies the condition of absolute stability in rudder angle and rate saturation.

2. Plant model

In this application, the rudder serves as the actuator in a two output closed loop system with a block diagram shown in Fig. 1. Fin stabilizers are not considered in this paper. The rudder to yaw/roll plant model is taken from van der Klugt (1987). Transfer functions from rudder angle to roll and yaw angles, $G_r(s)$ and $G_y(s)$, respectively, are given below

$$G_r(s) = \frac{0.3381s - 0.0169}{10s^3 + 2.18s^2 + 4.087s + 0.3969}, \quad (1)$$

$$G_y(s) = \frac{0.2106s + 0.05694}{s(16.67s^2 + 11.67s + 1)}. \quad (2)$$

The roll plant frequency response is shown in Fig. 2. The right-half plane zero at $0.05\,\mathrm{rad\,s^{-1}}$ has the capacity to complicate the roll controller design, and to deliver large closed loop sensitivity (magnitude of $1/(1+T(s))$ where $T(s)$ is the return ratio) at low frequency (Maciejowski, 1989). As the roll and yaw plants are coupled, there must be sufficient frequency separation in the individual control loops.

3. Rudder model

The simplified mathematical model of the rudder control loop described in van Amerongen (1982) is used in this paper. A

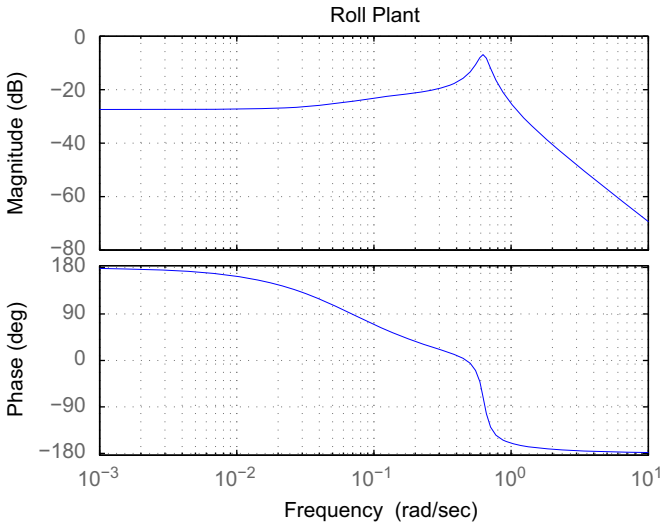

Fig. 2. Roll plant frequency response.

diagram of this system is shown in Fig. 3, and a good description of the steering machine dynamics is given in Fossen (1994).

The rudder is limited in angle, and the hydraulic steering machine is limited in rate, the effects of which are modeled as saturations (rudder limiter and rudder rate limiter, respectively) in Fig. 3. These saturations limit performance and potentially threaten the stability of the feedback system. In this paper, the angle limit is $35^\circ\,\mathrm{s^{-1}}$. Three rate limits are considered (10, 15, and $20^\circ\,\mathrm{s^{-1}}$).

4. Disturbance model

Roll and yaw disturbances by waves are modeled using the 2nd-order approximation of the Pierson–Moskowitz spectrum (Fossen, 1994; Laudval & Fossen, 1998; Pierson & Moskowitz,

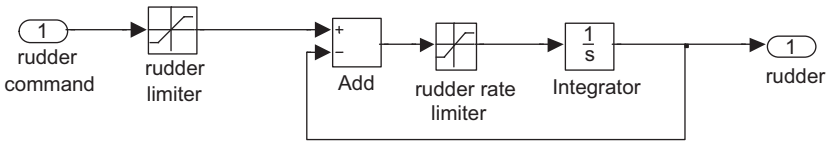

Fig. 3. Simplified rudder model with angle and rate limits.

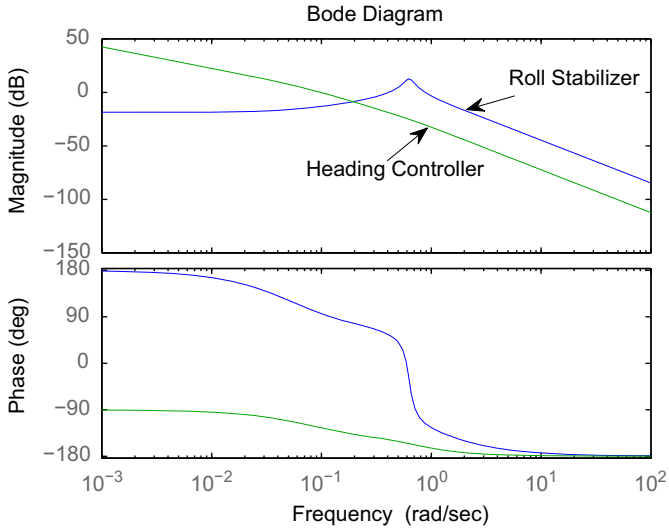

Fig. 4. Heading and roll controller return ratios.

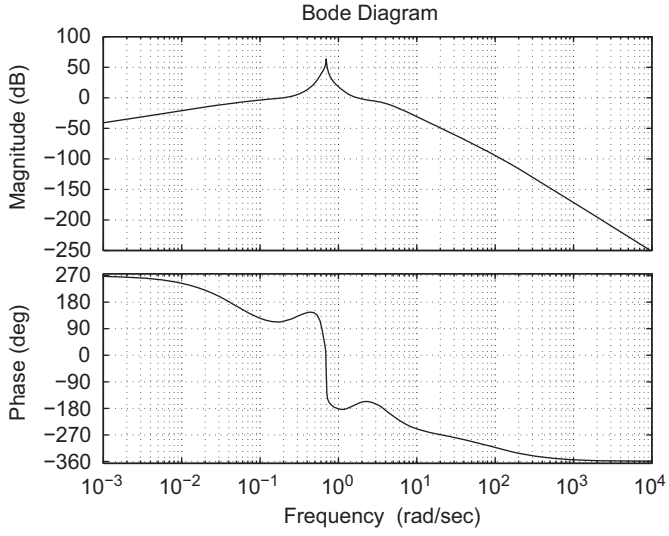

Fig. 5. High-order roll control return ratio.

1963; Saelid et al., 1983). Wave disturbances are

$$\omega_o(s) = h(s)\omega_i(s), \tag{3}$$

where $\omega_i(s)$ is Gaussian white noise. The filter is

$$h(s) = \frac{K_w s}{s^2 + 2\zeta_0\omega_0 s + \omega_0^2}, \tag{4}$$

where ω_0, ζ_0 and K_w are the dominate wave frequency, the damping coefficient and the wave strength coefficient, respectively.

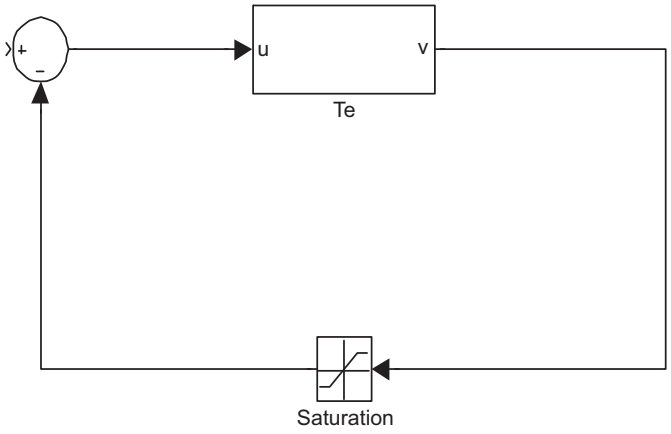

Fig. 6. Feedback connection of rudder saturation and the equivalent system.

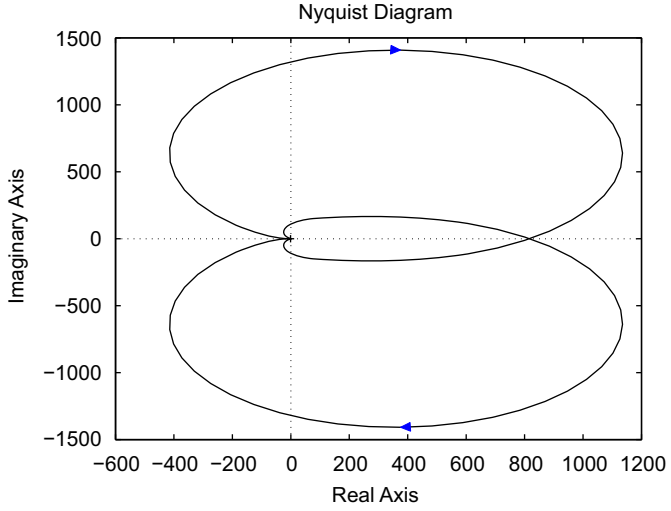

Fig. 7. Nyquist plot of high-order rudder roll stabilizer return ratio.

5. Heading control and low-order roll stabilizer

The return ratios of the heading and low-order roll controllers are shown in Fig. 4. These are designed to provide zero steady state error to the step heading command, and to achieve good heading track and roll reduction without saturating the rudder. The controllers are similar to those found in Laudval and Fossen (1998), where pole placement on the decoupled roll and yaw plants (rudder-induced sway is assumed to be zero) to find the heading and roll stabilization controllers.

6. Rudder roll stabilization controller

Three principal design issues are considered for the new roll stabilization controller. First, the wave disturbance spectrum is

concentrated in the decade from 0.1 to 1 rad s^{-1}. This, plus the fact that the actuator is not very effective in frequencies higher than 1 rad/s, suggests that the maximum available feedback (defined as the magnitude of $1+T(s)$ where $T(s)$ is the return ratio) should be applied in this interval. Second, the coupled yaw and roll plants require frequency separation between the heading and the roll stabilization controllers. The new roll controller will be designed to cross 0 dB at no less than 0.2 rad s^{-1}, which is the best case scenario. The third consideration is the non-minimum phase zero in the roll plant. It is fortunate that this zero is two octaves lower in frequency than the minimum first crossover frequency, as its phase contribution is only about 105° at 0.2 rad s^{-1}.

An 8th-order roll stabilizing controller is designed with these three issues taken into consideration. Loop shaping is used to provide large feedback over the interval 0.1−1 rad s^{-1}. The gain, zeros and poles for the compensator C_r are $K=79\,433$, $s_z=(0,\ -0.6000\pm1.3748i,\ -0.1800\pm0.2400i,\ -1.200,-0.5000)$, and $s_p=(-0.05,\ -2.400\pm3.624i,\ -0.6000\pm0.8000i,\ 0.0050\pm0.7000i,-100)$. The low frequency poles and zeros are spaced for a more aggressive roll-up/roll-off than is available with low-order compensation. A lead is applied to boost the phase at the second crossover. The simple pole at 100 rad s^{-1} reduces loop gain at high frequency and provides a strictly proper compensator transfer function. The zero at the origin provides a bandpass return ratio for the RRS controller. Fig. 5 shows the return ratio of the 8th-order roll controller.

7. Nonlinear compensator with multiple feedback paths for feedback transformation with multiple saturations

If a nonlinear element $\psi(t,v)$ satisfies the sector condition and the system can be expressed as a feedback connection of the element and a linear system T_e as shown in Fig. 6, then the Popov criterion can be used to assess the absolute stability of the system (origin is asymptotically stable for all nonlinearities in the sector) (Khalil, 1996). This is a sufficient condition only. The saturation nonlinearity satisfies the sector condition $0\le v\psi(t,v)\le v^2$ for all time. The circle criterion, a specific case of the Popov criterion, states if system $T_e(s)$ is Hurwitz and the system $Z(s)=1+T_e(s)$ is strictly positive real, then the system is absolutely stable for this sector, and thus for the saturation nonlinearity. The second condition is equivalent to the Nyquist plot of $T_e(j\omega)$ lying to the right of the vertical line $Re[s]=-1$. The Nyquist plot of the 8th-order roll controller is shown in Fig. 7. Clearly the system does not satisfy the condition of AS in saturation. In addition, the controller is Nyquist-stable (the Nyquist plot crosses the negative real axis outside the unit circle and the closed loop system is stable). These systems lose stability when there is a reduction in loop gain.

7.1. Nonlinear dynamic compensation for a single saturation

Nonlinear compensation is applied to the 8th-order linear RRS to provide AS in rudder angle saturation. The nonlinear roll controller is shown in Fig. 8. A second system C_n is connected in feedback to the nominal roll controller C_r via a deadzone link (Lurie & Enright, 2000). The deadzone 0 interval is the same as the linear interval of the actuator angle saturation. The return ratio for small signals is that shown in Fig. 5. For large signals (values where the output of the deadzone approaches that of the output of C_r), the feedback connection of C_r and C_n is the loop

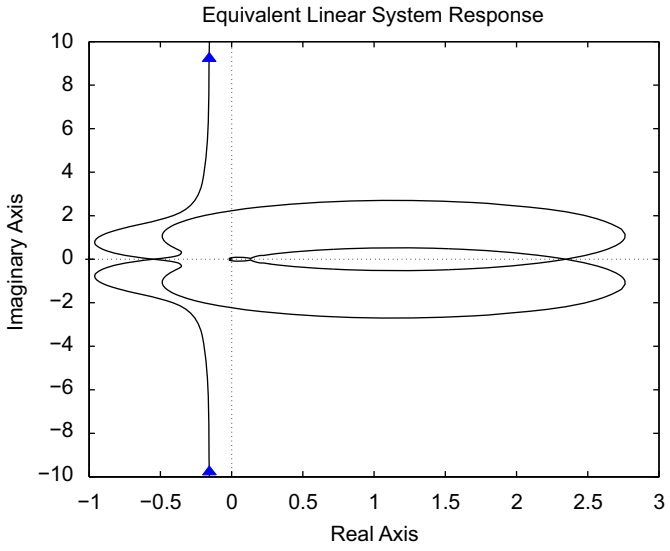

Fig. 9. $T_e(s)$ for high-order RRS with NDC and heading control.

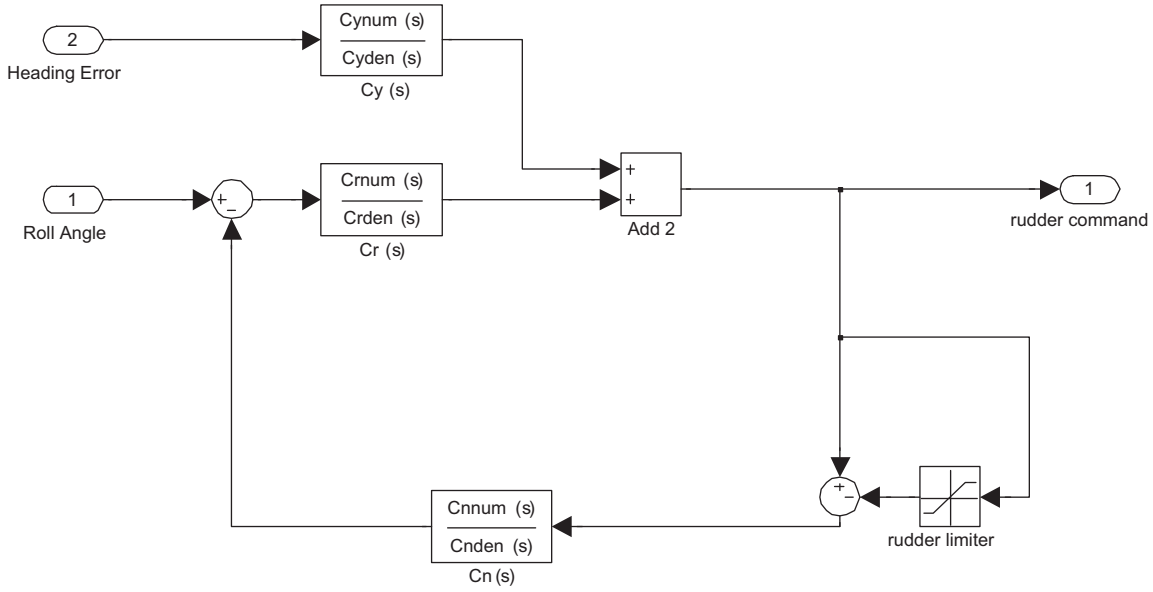

Fig. 8. Heading controller and RRS with NDC.

compensator C_{rl}. Given the desired large signal compensator transfer function C_{rl}, C_n is the following:

$$C_n(s) = \frac{C_r(s) - C_{rl}(s)}{C_r(s)C_{rl}(s)}. \tag{5}$$

The large signal compensator is chosen as $C_{rl} = 17.22s + 2.75$, which is the same controller found using pole placement in Fossen (1994). This compensator results in a loop transmission with less magnitude and shallower slopes than the small signal compensator. The goal here is to retain stability in the presence of saturation. The actuator and compensator saturations are identical, so the rudder angle saturation can be shown in feedback with the equivalent system (Lurie & Enright, 2000)

$$T_e(s) = \frac{C_r(s)P_r(s) + C_y(s)P_y(s) - C_r(s)C_n(s)}{1 + C_r(s)C_n(s)}, \tag{6}$$

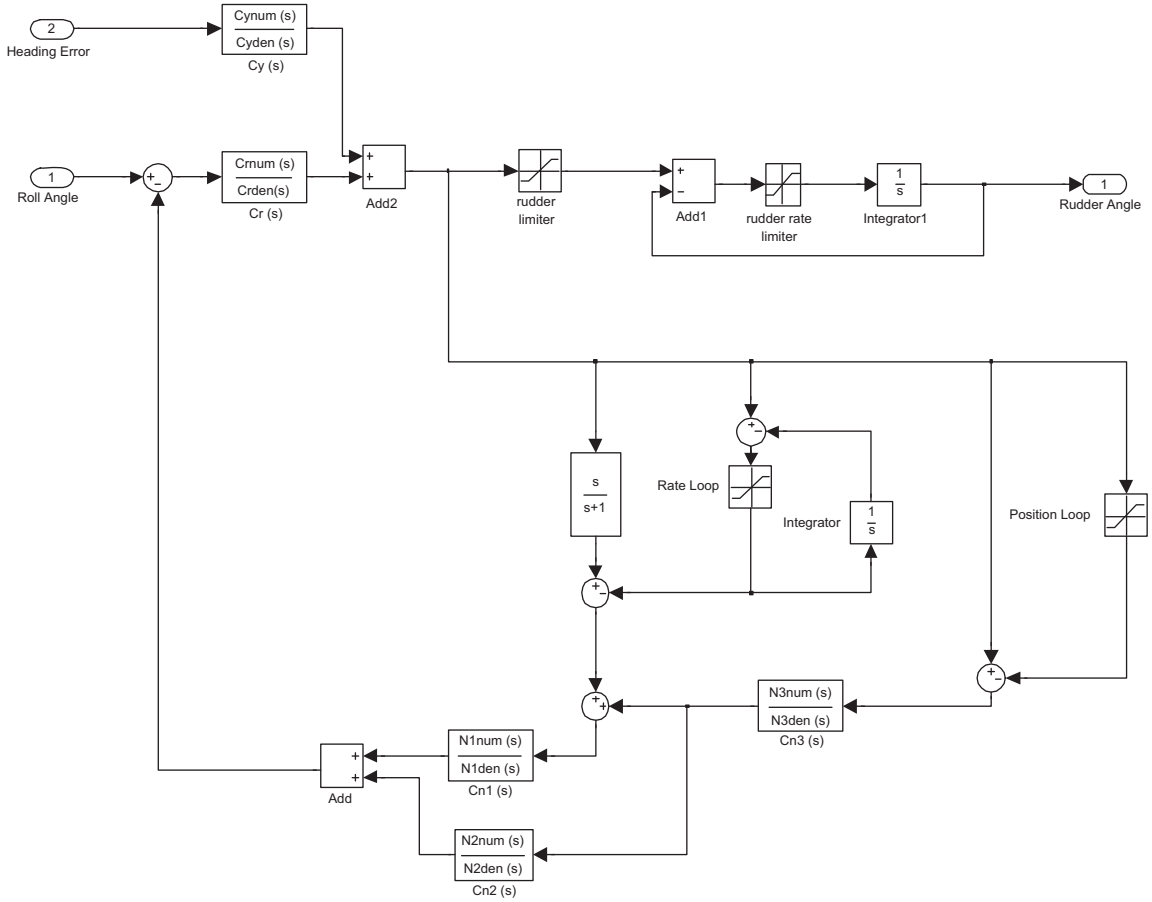

Fig. 10. Heading control and RRS with multiple feedback path NDC.

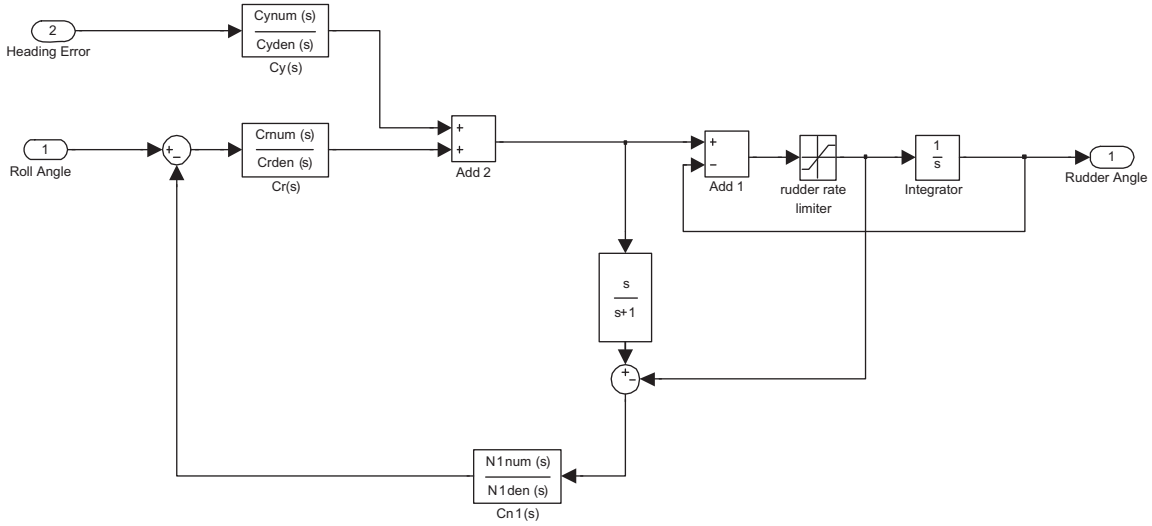

Fig. 11. Equivalent RRS compensator in the rate saturation condition.

where $C_y(s)$ is the PD heading control compensator, $P_r = G_r(1/(s+1))$ and $P_y = G_y(1/(s+1))$. The Nyquist plot of $T_e(s)$ is shown in Fig. 9. The plot lies to the right of $Re[s] = -1$, and thus the controller satisfies the circle criterion.

7.2. Nonlinear dynamic compensation for multiple saturations

The high-order controller with NDC applied to the rudder roll stabilization controller is AS only if the rudder is not rate saturated. Unfortunately, rate saturation is a key limitation in this application, especially for rudder steering machines on larger vessels. A new scheme is presented in this section that provides AS for rudder angle and rudder rate saturation. A block diagram of the controller is shown in Fig. 10. The saturation links in the NDC called "rate loop" and "position loop" are identical to the saturations "rudder rate limiter" and "rudder limiter" in the rudder model, respectively. In rudder rate saturation (no angle saturation), the equivalent compensator is shown in Fig. 11 which when connected to the plant gives the structure shown in Fig. 6 and AS analysis of the system can be performed. The equivalent linear system connected to the saturation nonlinearity is

$$T_{e_r}(s) = \frac{1 + G_r(s)C_r(s) + G_y(s)C_y(s) - C_r(s)C_{n_1}(s)\left(\dfrac{s^2}{s+1}\right)}{s\left(1 + C_r(s)C_{n_1}(s)\left(\dfrac{s}{s+1}\right)\right)}. \quad (7)$$

Transfer function C_{n_1} is chosen such that $T_{e_r} = T_e$ (Fig. 9), and thus the system is AS for the rudder rate saturation.

In rudder angle saturation (no rate saturation), the equivalent compensator is shown in Fig. 12. The saturation limits are identical to the rudder angle limits. This system connected to the plant yields the feedback connection to the saturation nonlinearity, and AS analysis is possible

$$T_{e_a}(s) = \frac{P_r(s)C_r(s) + P_y(s)C_y(s) - N_c(s)C_r(s)}{1 + N_c(s)C_r(s)}, \quad (8)$$

where $P_r(s) = G_r(s)(1/(s+1))$, $P_y(s) = G_y(s)(1/(s+1))$, and $N_c = C_{n_3}(C_{n_1} + C_{n_2}) = C_n$. The structure of N_c is chosen because non-minimum phase zeros in C_{n_1} make the filter C_n/C_{n_1} unstable, thus a cascade of two filters is not feasible. With the selected N_c, $T_{e_a} = T_e$ (Fig. 9) and the system is AS for the rudder angle saturation.

With this multi-path NDC, the high performance Nyquist-stable rudder roll stabilizer is AS for angle and rate saturations. The last stability consideration is the condition of *simultaneous* angle and rate saturation. This case does not lend itself to AS analysis. As the Popov criterion only tests sufficient, this is not an indication of instability. Fig. 13 shows the Nyquist plot for the very large signal loop gain for the multi-path NDC RRS with heading

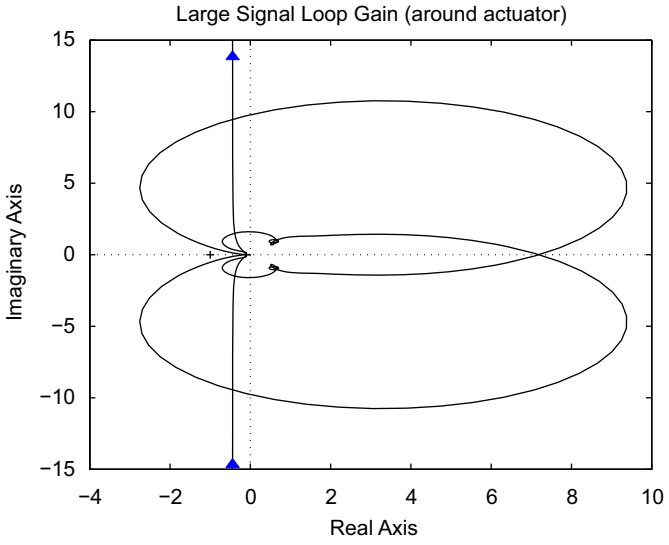

Fig. 13. Very large signal loop gain.

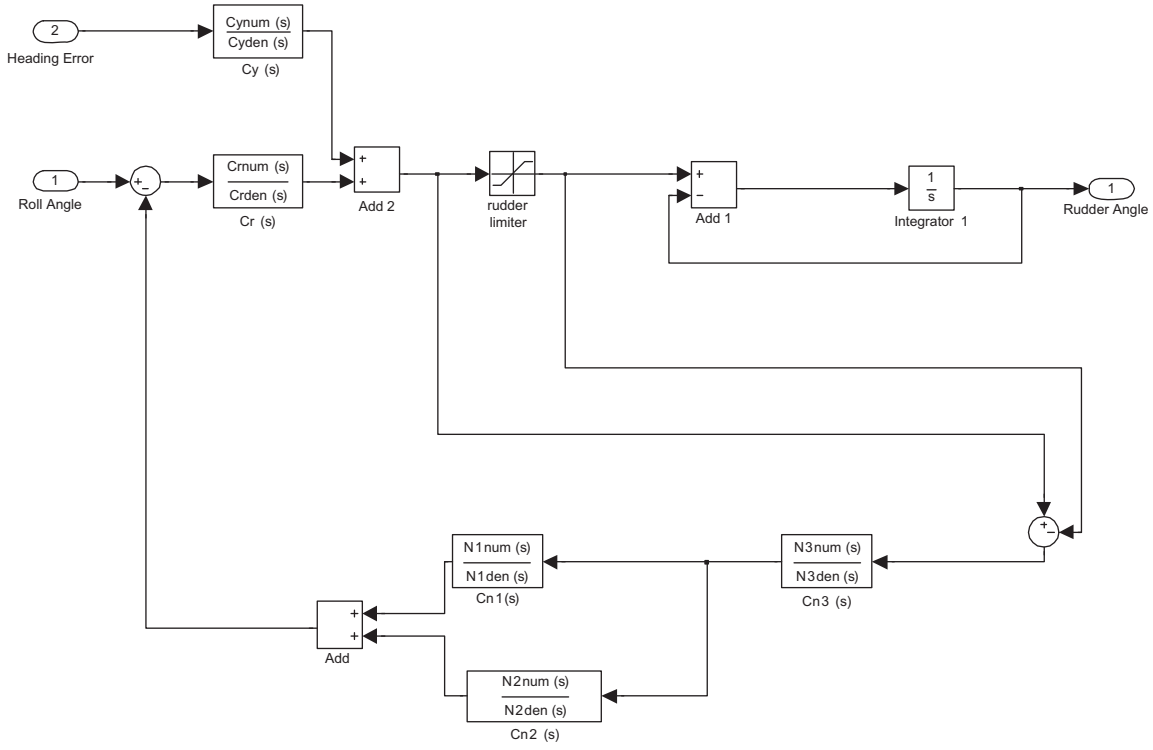

Fig. 12. Equivalent RRS compensator in angle saturation condition.

control around the rudder actuator. This is an approximation of the loop gain when the saturation paths in the NDC shown in Fig. 10 are negligible compared to the linear paths (the actuator is saturated in both rate and angle with large input signals). The critical point is not encircled if the plot collapses on the origin due to broadband saturation. No instabilities have been experienced in simulations where simultaneous saturations occur. While not rigorously proven, the results indicate stability retention in the simultaneous saturation condition.

Table 1
Roll reduction percentage for $\omega_0 = 0.3\,\text{rad}\,\text{s}^{-1}$.

	Rudder rate $= 20^\circ\,\text{s}^{-1}$	*Rudder rate* $= 15^\circ\,\text{s}^{-1}$	*Rudder rate* $= 10^\circ\,\text{s}^{-1}$
PD	44	44	42
HO + NDC	57	40	*x*
HO + multi−path NDC	61	56	48

Table 2
Roll reduction percentage for $\omega_0 = 0.5\,\text{rad}\,\text{s}^{-1}$ ("*x*" indicates oscillation).

	Rudder rate $= 20^\circ\,\text{s}^{-1}$	*Rudder rate* $= 15^\circ\,\text{s}^{-1}$	*Rudder rate* $= 10^\circ\,\text{s}^{-1}$
PD	68	68	65
HO + NDC	89	47	*x*
HO + multi−path NDC	87	84	72

Table 3
Roll reduction percentage for $\omega_0 = 0.7\,\text{rad}\,\text{s}^{-1}$ ("*x*" indicates oscillation).

	Rudder rate $= 20^\circ\,\text{s}^{-1}$	*Rudder rate* $= 15^\circ\,\text{s}^{-1}$	*Rudder rate* $= 10^\circ\,\text{s}^{-1}$
PD	68	68	65
HO + NDC	72	45	*x*
HO + multi−path NDC	90	86	84

Table 4
Roll reduction percentage for $\omega_0 = 0.9\,\text{rad}\,\text{s}^{-1}$ ("*x*" indicates oscillation).

	Rudder rate $= 20^\circ\,\text{s}^{-1}$	*Rudder rate* $= 15^\circ\,\text{s}^{-1}$	*Rudder rate* $= 10^\circ\,\text{s}^{-1}$
PD	31	30	22
HO + NDC	35	31	*x*
HO + multi−path NDC	72	65	67

8. RRS with multi-path NDC performance

The efficacy of the roll stabilizer is shown in computer simulations. Three RRS will be compared: low-order (PD), Nyquist-stable control with angle saturation NDC, and Nyquist-stable control with multi-path NDC. The PD heading controller described previously is used in conjunction with all three RRS systems. Three rudder rate limits are considered: 20, 15 and $10^\circ\,\text{s}^{-1}$. The wave model defined in Section 4 is employed using $K_w = 2.0$, $\omega_0 = 0.3, 0.5, 0.7, 0.9\,\text{rad}\,\text{s}^{-1}$ and $\zeta = 0.1$. A quantitative measure of the relative performance is provided by the roll reduction percentage defined by Oda et al. (1992)

$$\textit{roll reduction} = \frac{AP - RRCS}{AP} \times 100, \tag{9}$$

where *AP* is the standard deviation of roll rate with the heading controller on, RRS off, and *RRCS* the standard deviation of roll rate with both the heading and the RRS on. Tables 1–4 show the roll reductions for the PD controller shown in Fig. 4, high-order controller with rudder angle NDC only (HO + NDC), and high-order controller with multi-path NDC (HO + multi−path NDC).

The multi-path NDC system provides superior performance down to $10^\circ\,\text{s}^{-1}$ with the exception of a slight inferiority to HO + NDC with the fastest rudder. The enhanced performance is the result of large feedback in the linear condition, and a smooth transition to a less aggressive loop shape in either rudder angle or rate saturation.

The high-order controller with a single NDC feedback path (HO + NDC) is prone to oscillations triggered by rudder rate saturations that substantially reduce the roll reduction. This characteristic is increasing problematic as rudder speeds decrease,

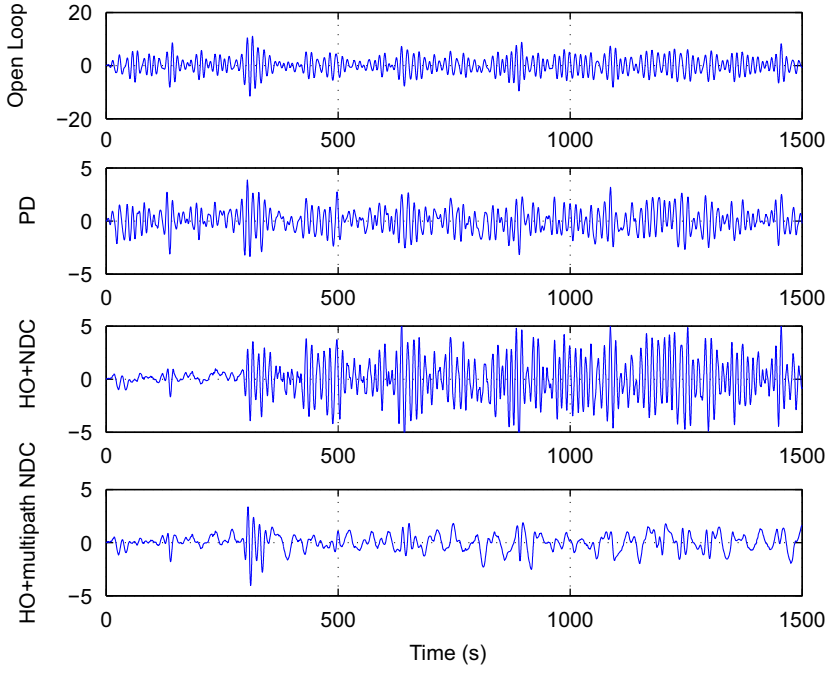

Fig. 14. Roll angles.

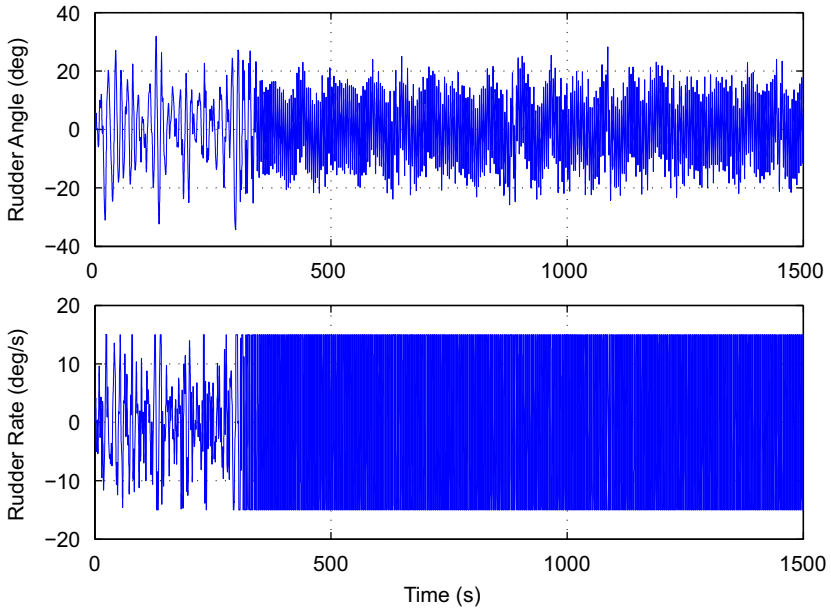

Fig. 15. Rudder angle/rate with closed loop angle only NDC.

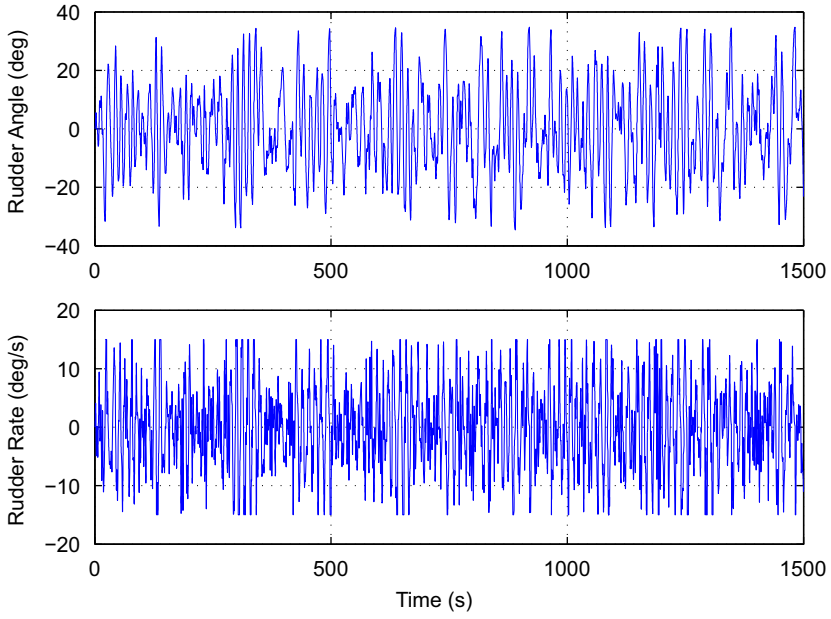

Fig. 16. Rudder angle/rate with closed loop multi-path NDC.

as indicated in the roll reduction tables. Fig. 14 shows the roll angles in open loop, closed PD roll stabilizer, closed HO + NDC and closed HO+ multi-path NDC with the $15^\circ\,s^{-1}$ rudder. The heading controller is closed in all three cases, with a heading command of 0. The disturbance event at approximately 310 s causes oscillation in the high-order controller with rudder angle NDC only, resulting in poor roll reduction performance. Fig. 15 shows the rudder angle and rates for this controller, where the rudder oscillations are evident. The rudder angle and rate signals for the same conditions are shown for the multi-path NDC controller in Fig. 16. It is noted that in contrast to the high-order controller with angle only NDC, this system does not oscillate. The angle and rate summing junction outputs are shown in Fig. 17 ($15^\circ\,s^{-1}$ rudder). There is saturation when these functions have nonzero values. The figure shows that both rudder angle and rate saturations occur over the 1500 s time interval.

8.1. Roll/yaw controller interaction

Interaction between the yaw and roll axis interaction is a critical issue for the RRS, as insufficient frequency separation of the controllers results in poor performance. Particular attention must be applied when using the simplified ship dynamics model of Van der Klugt, as only the most critical coupling terms are included. The effect of the multi-path NDC RRS system on the heading angle is tested by comparing the responses with the yaw controller and the RRS closed to those with only the yaw

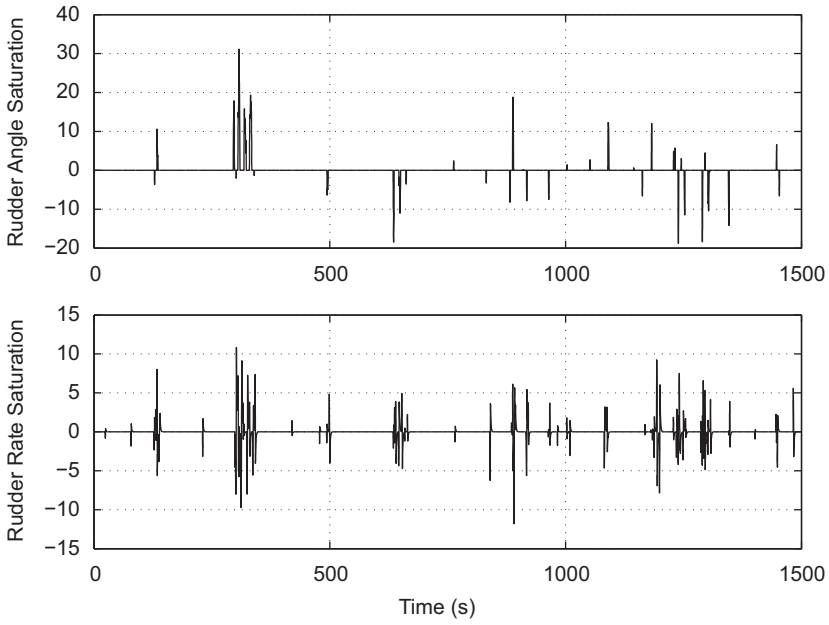

Fig. 17. Multi-path NDC deadzone outputs.

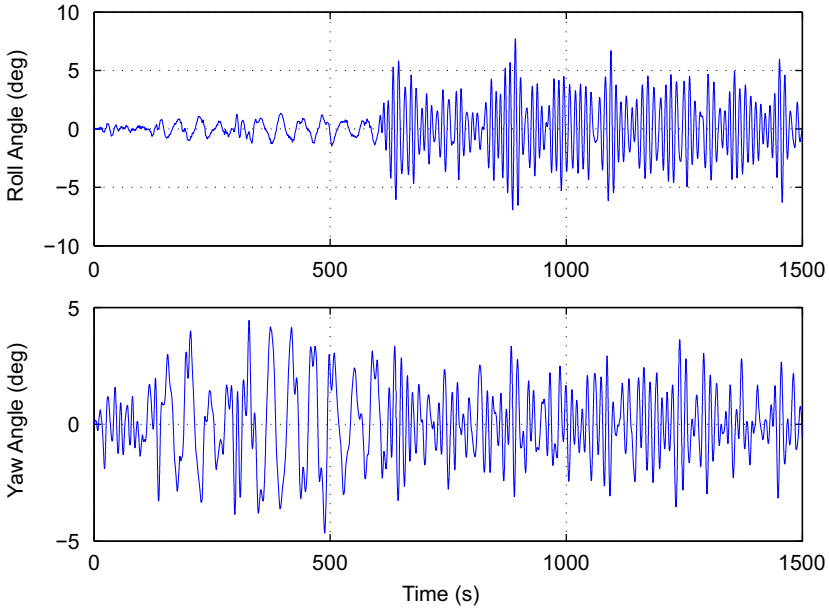

Fig. 18. Roll and yaw angles with multi-path NDC and $20^{\circ}\,s^{-1}$ rudder. The RRS loop is opened at 600 s.

controller closed. The fastest and slowest rudders are compared with a wave frequency of $\omega_0 = 0.5\,\mathrm{rad/s}$ in Figs. 18 and 19. It is noted that the system with the slower rudder, being in the saturated condition more frequently, while stable, shows more interaction between the two loops.

9. Conclusions and future work

An 8th-order rudder roll stabilization control system with multiple path nonlinear dynamic compensation is presented. Rudder-induced sway coupling, a non-minimum phase roll plant, and an actuator prone to position and rate saturation make the control design very challenging, requiring careful shaping of the loop gain to achieve good performance. The linear controller is Nyquist-stable, requiring a nonlinear compensator to smoothly transition to a less aggressive loop gain in the saturated condition. The novel multi-path NDC provides absolute stability in either the angle or the rate saturated condition, and unlike the angle only NDC is not prone to oscillations triggered by rudder rate saturation. This unique design feature allows the implementation of the high-order controller with superior roll reduction than low-order linear controllers on slower steering mechanisms used on larger vessels. The implementation of nonlinear dynamic compensation allows the application of more feedback than linear controllers, while retaining stability in saturation.

Retaining stability in the presence of actuator saturations is not the only consideration. Indeed, the performance advantage of the high-order controller decreases if the actuator is frequently saturated. Future work will include and investigation of adaptive

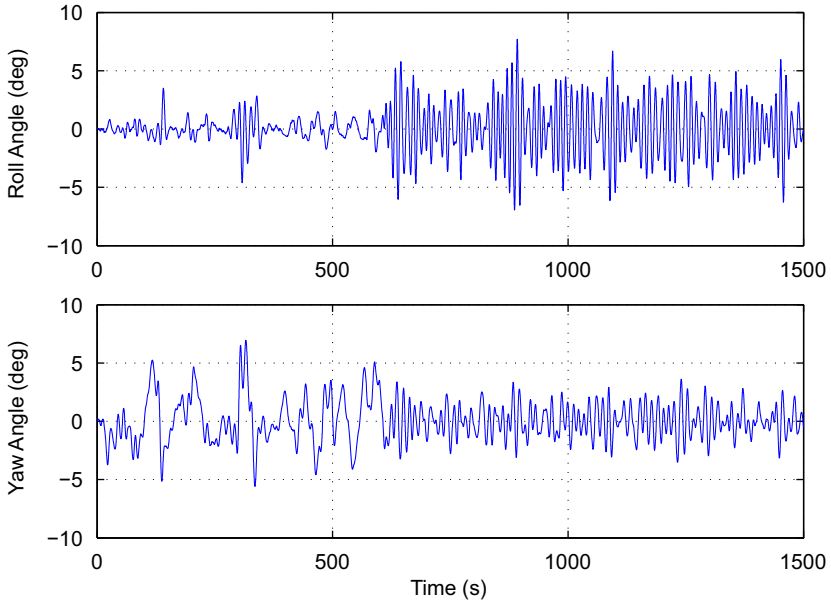

Fig. 19. Roll and yaw angles with multi-path NDC and $10^{\circ}\,s^{-1}$ rudder. The RRS loop is opened at 600 s.

algorithms for the linear and nonlinear compensators to reduce saturation frequency. Future investigation will also include the development of a multi-path NDC gain scheduling algorithm for variable ship states. Yaw/roll reduction controller frequency separation problem will be a particularly interesting aspect of this problem.

Acknowledgments

The author would like to thank Luke J. Hollmann at Notre Dame and James Nelson at the University of Wyoming for their assistance in developing figures, and Dr. Boris J. Lurie at NASA's Jet Propulsion Laboratory for his invaluable instruction and friendship.

References

Alarcin, F. (2007). Internal model control using neural network for ship roll stabilization. *Journal of Marine Science and Technology*, *15*(2), 141–147.

Engeln, A., Koshkouei, A., Roberts, G., & Burnham, K. (2004). *Ship roll stabilization via switched control system. Control 2004*. UK: University of Bath.

Faltinsen, O. M. (1990). *Sea loads on ships and offshore structures*. Cambridge, MA: Cambridge University Press.

Fossen, T. (1994). *Guidance and control of ocean vehicles*. New York, NY: Wiley.

Goodwin, G., Perez, T., Seron, M., & Tzeng, C. (2000). On fundamental limitations for rudder roll stabilization of ships. In *Proceedings of the 39th IEEE conference on decision and control* (pp. 4705–4710).

Khalil, H. (1996). *Nonlinear systems*. Upper Saddle River, NJ: Prentice-Hall.

Laudval, T., & Fossen, T. (1998). Rudder roll stabilization of ships subject to input rate saturation using a gain scheduled control law. In *IFAC conference on control applications in marine systems* (pp. 121–127).

Lurie, B., & Enright, P. (2000). *Classical feedback control*. New York, NY: Marcel Dekker.

Maciejowski, J. (1989). *Multivariable feedback design*. Wokingham, UK: Addison-Wesley.

Majecki, P., Katebi, R., & Grimble, M. (2006). Rudder roll stabilization with nonlinear GMV control. In *International control conference (ICC 2006)*. Glasgow, UK.

O'Brien, J. (2007). High order rudder roll stabilization controller with nonlinear compensation. In *Proceedings of the ASNE automation and control symposium*. Biloxi, MS, US.

Oda et al. (1992). Rudder roll stabilization control system through multivariable auto regressive model. In *Proceedings of the 3rd IFAC workshop on control applications in marine systems* (pp. 113–127).

Perez, T. (2005). *Ship motion control: Course keeping and roll stabilization using rudder and fins*. London, UK: Springer.

Perez, T., & Goodwin, G. (2007). Constrained predictive control of ship fin stabilizers to prevent dynamic stall. *Control Engineering Practice*, *16*(4), 482–494.

Pierson, W., & Moskowitz, L. (1963). A proposed spectral form for fully developed wind seas based on the similarity theory of S. A. Kitaigorodsku. US Naval Oceanographic Office Contract 62306-1042.

Roberts, G. (1993). A note on the applicability of rudder roll stabilization for ships. In *Proceedings of the American control conference* (pp. 2403–2407).

Saelid, S., Jenssen, N., & Balcen, J. (1983). Design and analysis for a dynamic positioning system based on Kalman filtering and optimal control. *IEEE Transactions on Automatic Control*, *28*(3), 331–339.

Sharif, M., Roberts, G., & Sutton, R. (1996). Final experimental results of full scale fin/rudder roll stabilization sea trials. *Control Engineering Practice*, *4*(3), 377–384.

Tzeng, C., & Wu, C. (2000). On the design and analysis of ship stabilizing fin controller. *Journal of Marine Science and Technology*, *8*(2), 117–124.

van Amerongen, J. (1982). *Adaptive steering of ships-A model reference approach to improved maneuvering and economical course keeping*. Ph.D. thesis, Delft University of Technology.

van der Klugt, P. (1987). *Rudder roll stabilization*. Ph.D. thesis, Delft University of Technology.